Secondorder asymptotic solution for laminar separation

S. A. Ragab and Ali H. Nayfeh

Citation: Physics of Fluids (1958-1988) **23**, 1091 (1980); doi: 10.1063/1.863111
View online: http://dx.doi.org/10.1063/1.863111
View Table of Contents: http://scitation.aip.org/content/aip/journal/pof1/23/6?ver=pdfcov
Published by the AIP Publishing

Second-order asymptotic solution for laminar separation

S. A. Ragab and Ali H. Nayfeh

Engineering Science and Mechanics Department, Virginia Polytechnic Institute and State University, Blacksburg, Virginia 24061

(Received 22 February 1979; accepted 31 January 1980)

The method of matched asymptotic expansions is used to obtain a second-order triple-deck solution for the case of constant wall temperature. It includes the problem of an adiabatic wall as a special case. The theory is applied to the case of a supersonic flow over a compression ramp with laminar separation. A numerical procedure is presented for solving the lower-deck equations by using the Crank–Nicolson finite-difference scheme. A modification of the boundary conditions for an adiabatic wall made it possible to solve for the total second-order solution instead of solving for the different orders in succession. Sample results and comparisons with other solutions are presented. The region of separation predicted by the second-order theory is larger than that predicted by the first-order theory. Moreover, for the case of cooled walls, the second-order theory predicts negative temperatures and densities, depending on the Reynolds number and the degree of cooling, thus indicating a breakdown of the theory.

I. INTRODUCTION

We consider a disturbance introduced into the boundary-layer at a point x_p^* far from the leading edge of a plate. The disturbance may be due to an incident shock wave, the start of a compression ramp, a sudden change in the boundary conditions on the wall, etc.

In his study of the upstream propagation of small disturbances in shock-wave boundary-layer interactions, Lighthill[1] showed that, in the limit of infinite Reynolds number, the flow field exhibits a unique substructure. Stewartson and Williams,[2] Neiland,[3] and Messiter[4] independently developed a rational theory, termed the triple-deck theory, to describe the substructure noted by Lighthill. Their theory shows that the proper streamwise length scale is $O(\epsilon^3 x_p^*)$, where ϵ is defined by

$$\epsilon = \mathrm{Re}^{-1/8}$$

and Re is a characteristic Reynolds number defined by

$$\mathrm{Re} = \zeta_\infty^* U_\infty^* x_p^* / \mu_\infty^* .$$

Upstream of the interaction region, the boundary layer is the familiar Prandtl boundary layer. In the interaction region, the flow is described by three layers or decks as shown schematically in Fig. 1. The main (middle) deck is the displaced Prandtl boundary layer; its thickness is $O(\epsilon^4 x_p^*)$. The disturbances in this deck are inviscid but rotational. The thickness of the upper deck is $O(\epsilon^3 x_p^*)$ and the disturbances in this deck are inviscid and irrotational. The thickness of the lower deck is $O(\epsilon^5 x_p^*)$. To first order, the equations governing the total flow in this deck are the incompressible boundary-layer equations. The result of matching these decks to first order is the solution of the incompressible boundary-layer equations subject to novel boundary conditions. Stewartson[5] gave a comprehensive survey of the triple-deck theory.

Jenson *et al.*,[6] Rizzetta,[7] and Rizzetta *et al.*[8] developed a numerical scheme to solve the first-order triple-deck problem for the case of supersonic and hypersonic flows past corners. They formulated the problem in terms of the shear stress and added an unsteady term to the momentum equation. Then, they determined steady-flow solutions as the long-time limit of the solutions of the unsteady problem. Their numerical scheme is second-order accurate in Δz, while it is first-order accurate in Δt and Δx, except that the compatibility condition at the wall is second-order accurate in Δx, where t is time and x and z are the dimensionless lower-deck variables along and normal to the plate. Consequently, their numerical scheme is sensitive to the value of Δx and they had to linearly extrapolate their results to a zero mesh size. One of the purposes of the present paper is to present a numerical scheme based on that of Rizzetta[7] and Rizzetta *et al.*[8] that is second-order accurate in Δx and Δz, while it is first-order accurate in Δt. Numerical results show that the solution is weakly dependent on Δx.

Werle and Vatsa[9] developed a numerical scheme based on interacting boundary layers for the calculation of viscous-inviscid interactions in supersonic flows. Their results for flows over compression ramps are in good agreement with available experimental data and with the Navier–Stokes solutions of Carter.[10] Burgraf *et al.*[11] compared the triple-deck results with the interacting boundary-layer results for a number of Reynolds numbers. As $\mathrm{Re} \to \infty$, the triple-deck and interacting boundary-layer results are in good agreement; but, as Re decreases, the two results deviate more and more indicating a weakness in the first-order triple-deck theory.

To first order, the governing equations in the lower deck are independent of the thermal conditions on the wall; they are valid for adiabatic as well as constant wall temperatures. Brown and Williams[12] extended the triple-deck theory to second order. Now, the governing equations depend on the thermal condition on the wall, and their analysis is valid only for adiabatic walls. They determined the pressure and its gradient at the point of separation in the free-interaction problem. No numerical results concerning the flow field inside the separation bubble were presented in their paper. A second purpose of the present paper is to adapt the second-order accurate numerical scheme to solve the second-order triple-deck equations for the case of flow over compression ramps. Our numerical

 0031-9171/80/061091-10$00.90

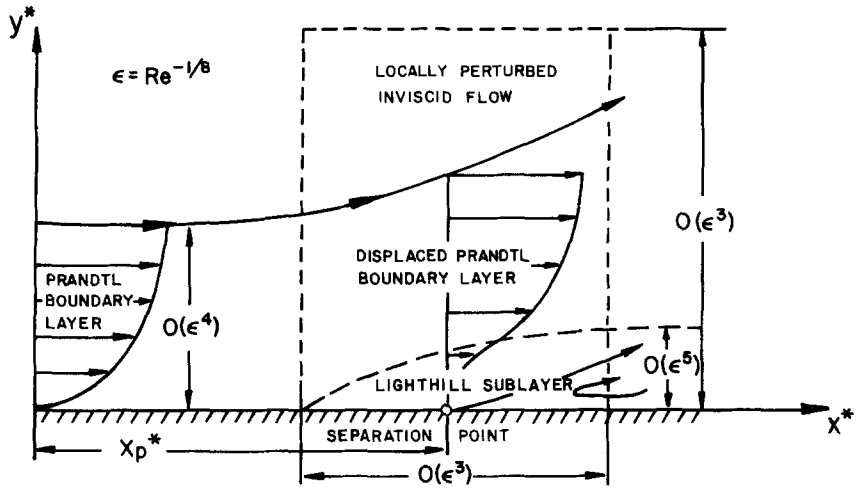

FIG. 1. The triple-deck structure.

second-order corrections to the pressure and its derivative at the separation point are considerably different from those of Brown and Williams.[12] Moreover, at finite values of Re, the second-order triple-deck results show even greater differences from the interacting boundary-layer results than the first-order triple-deck results.

The third and principal purpose of the present paper is to develop the governing equations for the second-order problem for a nonadiabatic wall. The second-order theory is used to calculate the flow past a compression ramp with small-bubble separation. The numerical procedure used to solve the second-order triple-deck problem for the case of adiabatic walls is adapted to handle the second-order triple-deck problem for the case of nonadiabatic walls. Numerical results for the case of cooled walls show that the density and temperature may be negative unless the Reynolds number is very large. This indicates a breakdown in the matched asymptotic version of the triple-deck theory. The breakdown is a result of expanding the basic state in powers of the transverse coordinate.

II. THE BASIC STATE

We consider a compressible, viscous flow past a flat plate at zero incidence as in Fig. 1. The fluid is assumed to be Newtonian with a coefficient of viscosity μ^* given by Chapman's law

$$\mu^*/\mu_\infty^* = C(T^*/T_\infty^*) , \tag{1}$$

where C is a constant. Furthermore, the wall is assumed to be kept at a constant temperature T_w^* and the Prandtl number Pr is taken to be unity.

The velocity profile $U^*(x^*, y^*)$ is determined by a Blasius solution which is suitably generalized for compressible flow. Hence,

$$U^*(x^*, y^*) = U_\infty^* f(\eta) , \tag{2}$$

where $f(\eta)$ is the well-known Blasius profile and

$$\eta = (\mathrm{Re}_x/2C)^{1/2} (\bar{y}/x^*) , \tag{3}$$

with

$$\bar{y} = \int_0^{y^*} \frac{\rho^*(x^*, y^*)}{\rho_\infty^*} dy^*, \quad \mathrm{Re}_x = \frac{\rho_\infty^* U_\infty^* x^*}{\mu_\infty^*} . \tag{4}$$

The temperature profile $T^*(x^*, y^*)$ is obtained from the energy equation as

$$T^*(x^*, y^*) = T_\infty^* \left[1 + \left(\frac{T_w^*}{T_\infty^*} - 1\right)(1 - f'^2) + \xi \frac{T_w^*}{T_\infty^*} (1 - f')f'\right] , \tag{5}$$

where

$$\xi = T_{ad}^*/T_w^* - 1 , \tag{6}$$

and T_∞^*, T_w^*, and T_{ad}^* are the free-stream temperature, the wall temperature, and the adiabatic wall temperature, respectively. For an adiabatic wall, $\xi = 0$.

III. MATHEMATICAL FORMULATION

We superpose a small disturbance on the basic state. The small disturbance was shown in Ref. 2–4 to exhibit a triple-deck structure consisting of a lower deck, a main deck, and an upper deck.

The analysis of the disturbance in the main and upper decks is the same as that presented by Brown and Williams[12] for the case of thermally insulated walls. As mentioned in the Introduction, the disturbance in the main deck is inviscid but rotational. The solution in this deck is[12]

$$u/U_\infty^* = U(Y_m) + \epsilon u_1 + \epsilon^2 u_2 + \cdots , \tag{7}$$

$$v^*/U_\infty^* = \epsilon^2 v_1 + \epsilon^3 v_2 + \cdots , \tag{8}$$

$$\rho^*/\rho_\infty^* = R(Y_m) + \epsilon\rho_1 + \epsilon^2\rho_2 + \cdots , \tag{9}$$

$$(\rho^* - p_\infty^*)/\rho_\infty^* U_\infty^{*2} = \epsilon^2 p_2 + \epsilon^3 p_3 + \cdots , \tag{10}$$

where

$$u_1 = \frac{dU}{dY_m} A_1(X), \quad v_1 = -U \frac{dA_1}{dX} , \tag{11}$$

$$\rho_1 = \frac{dR}{dY_m} A_1(X), \quad p_2 = p_2(X) , \tag{12}$$

$$u_2 = M_\infty^2 p_2 \left[\frac{dU}{dY_m} \int_{Y_m}^{\infty} \left(\frac{1}{M^2} - \frac{1}{M_\infty^2} \right) dY_m + \left(1 - \frac{1}{M_\infty^2} \right) Y_m \frac{dU}{dY_m} - \frac{U}{M^2} \right] + \frac{1}{2} A_1^2 \frac{d^2U}{dY_m^2} + A_2 \frac{dU}{dY_m} , \tag{13}$$

$$v_2 = -M_\infty^2 U \frac{dp}{dX} \int_{Y_m}^{\infty} \left(\frac{1}{M^2} - \frac{1}{M_\infty^2} \right) dY_m - (M_\infty^2 - 1) U Y_m \frac{dp_2}{dX} - A_1 \frac{dA_1}{dX} \frac{dU}{dY_m} - U \frac{dA_2}{dX} , \tag{14}$$

$$\rho_2 = M_\infty^2 p_2 \left[\frac{dR}{dY_m} \int_{Y_m}^{\infty} \left(\frac{1}{M^2} - \frac{1}{M_\infty^2} \right) dY_m + \left(1 - \frac{1}{M_\infty^2} \right) Y_m \frac{dR}{dY_m} + R \right] + \frac{1}{2} A_1^2 \frac{d^2R}{dY_m^2} + A_2 \frac{dR}{dY_m} , \tag{15}$$

$$p_3 = \left(Y_m - \int_0^{Y_m} \frac{M_\infty^2 - M^2}{M_\infty^2} dY_m \right) \frac{d^2A_1}{dX^2} + p_3(X, 0), \tag{16}$$

$$x^* = x_p^* + \epsilon^3 X x_p^* , \quad y^* = \epsilon^4 Y_m x_p^* . \tag{17}$$

Here $M^2 = M_\infty^2 R U^2$, $p_3(X, 0)$ is a function of X to be determined in the course of the analysis, and $A_n(X) \to 0$ as $X \to -\infty$ in order that $u_n \to 0$ as $X \to -\infty$.

Note that the solution in the main deck contains four undetermined functions $A_1(X)$, $A_2(X)$, $p_2(X)$, and $p_3(X, 0)$. Two relations among these functions are provided by matching with the upper deck; hence, A_1 and A_2 can be expressed in terms of $p_2(X)$ and $p_3(X, 0)$ The latter functions are determined from matching with the lower deck.

The disturbance in the upper deck is inviscid, irrotational, and given by the Prandtl–Glauert equations. To second order, they are[12]

$$u^*/U_\infty^* = 1 + \epsilon^2 \hat{u}_2 + \epsilon^3 \hat{u}_3 + \cdots , \tag{18}$$

$$v^*/U_\infty^* = \epsilon^2 \hat{v}_2 + \epsilon^3 \hat{v}_3 + \cdots , \tag{19}$$

$$\rho^*/\rho_\infty^* = 1 + \epsilon^2 \hat{\rho}_2 + \epsilon^3 \hat{\rho}_3 + \cdots , \tag{20}$$

$$(p^* - p_\infty^*)/\rho_\infty^* U_\infty^{*2} = \epsilon^2 \hat{p}_2 + \epsilon^3 \hat{p}_3 + \cdots , \tag{21}$$

where

$$\hat{p}_n(X, Y_u) = -\hat{u}_n(X, Y_u) = F_n[X - (M_\infty^2 - 1)^{1/2} Y_u], \quad \hat{\rho}_n = M_\infty^2 \hat{p}_n , \tag{22}$$

$$\hat{v}_n(X, Y_u) = (M_\infty^2 - 1)^{1/2} F_n[X - (M_\infty^2 - 1)^{1/2} y_u], \tag{23}$$

$$y^* = \epsilon^3 Y_u x_p^* , \quad x^* = x_p^* + \epsilon^3 X x_p^* , \tag{24}$$

and $F_n \to 0$ as $\eta \to -\infty$.

Matching the main and upper decks yields

$$A_1(X) = -(M_\infty^2 - 1)^{1/2} \int_{-\infty}^{X} p_2 dX , \tag{25}$$

$$A_2(X) = -(M_\infty^2 - 1)^{1/2} \times \left((M_\infty^2 - 1)^{1/2} p_2 I + \int_{-\infty}^{X} p_3(X, 0) dX \right) , \tag{26}$$

where

$$I = \int_0^{\infty} \frac{M_\infty^2 - M^2}{M_\infty^2} dY_m = (2C)^{1/2} \frac{T_w^*}{T_\infty^*} (I_1 + \xi I_2) , \tag{27}$$

$$I_1 = \int_0^{\infty} (1 - f'^2) d\eta = 1.68638 ,$$
$$I_2 = \int_0^{\infty} (1 - f') f' d\eta = 0.46960 . \tag{28}$$

The main-deck solution, Eqs. (7)–(10), does not satisfy the conditions at the wall. To see this, we exhibit the behavior of the main-deck solution as $Y_m \to 0$. This behavior depends on the thermal condition at the wall. For a wall having a constant temperature,

$$u_1 = \frac{\alpha}{(2C)^{1/2}} \frac{T_\infty^*}{T_w^*} A_1 \left(1 - \frac{\alpha \xi}{(2C)^{1/2}} \frac{T_\infty^*}{T_w^*} Y_m + O(Y_m^2) \right) , \tag{29}$$

$$\rho_1 = A_1 \left[-\frac{\alpha \epsilon}{(2C)^{1/2}} \left(\frac{T_\infty^*}{T_w^*} \right)^2 + O(Y_m) \right] , \tag{30}$$

$$v_1 = -\frac{\alpha}{(2C)^{1/2}} \frac{T_\infty^*}{T_w^*} \frac{dA_1}{dx} \left(Y_m - \frac{\alpha \xi}{2(2C)^{1/2}} \frac{T_\infty^*}{T_w^*} Y_m^2 + O(Y_m^3) \right) , \tag{31}$$

$$u_2 = -2\xi \frac{T_w^*}{T_\infty^*} p_2 \log \frac{Y_m}{G} + (\alpha \phi - 2\xi) \frac{T_w^*}{T_\infty^*} p_2 - \frac{\alpha^2}{4C} \xi \left(\frac{T_\infty^*}{T_w^*} \right)^2 A_1^2 + \frac{\alpha}{(2C)^{1/2}} \frac{T_\infty^*}{T_w^*} A_2 + O(Y_m \log Y_m) , \tag{32}$$

$$\rho_2 = \frac{\xi G}{\alpha} p_2 \frac{1}{Y_m} + 2\xi^2 \log \frac{Y_m}{G} + O(1) , \tag{33}$$

$$v_2 = -\frac{G}{\alpha} \frac{T_w^*}{T_\infty^*} \frac{dp_2}{dX} + 2\xi \left(\frac{T_w^*}{T_\infty^*} \right) \frac{dp_2}{dX} Y_m \log \frac{Y_m}{G} - \alpha (2C)^{-1/2} \frac{T_\infty^*}{T_w^*} A_1 \frac{dA_1}{dX} + O(Y_m), \tag{34}$$

where $\alpha = f''(0) = 0.4696$, $G = (2C)^{1/2} T_w^*/T_\infty^*$,

$$\phi = -\left(1 - \frac{T_\infty^*}{T_w^*} \right) I_1 - \xi \left(2 - \frac{T_\infty^*}{T_w^*} \right) I_2 + \xi^2 I_3 + I_4 + 2\xi I_5, \tag{35}$$

$$I_3 = \int_0^{\infty} (1 - f') d\eta - \int_0^{\infty} (1 - f') f' d\eta = 0.7472 , \tag{36a}$$

$$I_4 = \int_0^{\infty} \left(\frac{1}{f'^2} - \frac{1}{\alpha^2 \eta^2} - 1 \right) d\eta = -3.663, \tag{36b}$$

$$I_5=\int_0^1\left(\frac{1}{f'}-\frac{1}{\alpha\eta}-1\right)d\eta+\int_1^\infty\left(\frac{1}{f'}-1\right)d\eta=-0.2994\ . \tag{36c}$$

Equations (29)–(34) involve expansions of U, dU/dY_m, and dR/dY_m in Taylor series in terms of Y_m, and hence, they are valid only for small values of Y_m. Consequently, the resulting solution breaks down, depending on the Reynolds number and the wall cooling. Further discussion is presented in Sec. V.

The appropriate scalings in this layer are

$$y^*=\epsilon^5 Y_1 x_p^*,\quad x^*=x_p^*+\epsilon^3 X x_p^*\ . \tag{37}$$

The order of magnitude of the variables in this deck can be inferred from the behavior of the solution in the main deck as $Y_m\to 0$; thus,

$$\frac{u^*}{U_\infty^*}=\epsilon\tilde{u},\quad \frac{v^*}{U_\infty^*}=\epsilon^3\tilde{v},\quad \frac{\rho^*}{\rho_\infty^*}=\tilde{\rho},\quad \frac{(p^*-p_\infty^*)}{\rho_\infty^* U_\infty^*}=\epsilon^2\tilde{p}\ . \tag{38}$$

It is convenient to introduce a transformation which renders the leading-order terms independent of the free-stream variables. Following Stewartson and Williams,[2] we let

$$X=C^{3/8}\lambda^{-5/4}(M_\infty^2-1)^{-3/8}(T_w^*/T_\infty^*)^{3/2}x\ , \tag{39a}$$

$$Y_1=C^{5/8}\lambda^{-3/4}(M_\infty^2-1)^{-1/8}(T_w^*/T_\infty^*)^{3/2}y, \tag{39b}$$

$$\tilde{p}=C^{1/4}\lambda^{1/2}(M_\infty^2-1)^{-1/4}p(x)\ , \tag{39c}$$

$$\tilde{\rho}=(T_\infty^*/T_w^*)\rho(x,y)\ , \tag{39d}$$

$$\tilde{u}=C^{1/8}\lambda^{1/4}(M_\infty^2-1)^{-1/8}(T_w^*/T_\infty^*)^{1/2}u(x,y)\ , \tag{39e}$$

$$\tilde{v}=C^{3/8}\lambda^{3/4}(M_\infty^2-1)^{1/8}(T_w^*/T_\infty^*)^{1/2}v(x,y)\ , \tag{39f}$$

$$A_1(X)+\epsilon A_2(X)=C^{5/8}\lambda^{-3/4}(M_\infty^2-1)^{-1/8}(T_w^*/T_\infty^*)^{3/2}[A(x)+\epsilon B(x)]\ . \tag{39g}$$

Under this transformation, the governing equations become

$$\rho\left(u\frac{\partial u}{\partial x}+v\frac{\partial u}{\partial y}\right)=-\frac{\partial p}{\partial x}+\frac{\partial}{\partial y}\left(\frac{1}{\rho}\frac{\partial u}{\partial y}\right)\ , \tag{40}$$

$$\frac{\partial p}{\partial y}=0\ , \tag{41}$$

$$\frac{\partial \rho u}{\partial x}+\frac{\partial \rho v}{\partial y}=0\ , \tag{42}$$

$$u\frac{\partial \rho}{\partial x}+v\frac{\partial \rho}{\partial y}=\rho\frac{\partial}{\partial y}\left(\frac{1}{\rho^3}\frac{\partial \rho}{\partial y}\right)\ , \tag{43}$$

where terms of $O(\epsilon^2)$ are neglected. Equation (41) gives $p=p(x)$.

The solution in this deck must match with the solution in the main deck. Substituting Eqs. (29) and (32) into Eq. (7) and expanding $U(Y_m)$ in Taylor series, we find that the matching condition gives

$$u\to y-\int_{-\infty}^x p\,dx-\omega_{20}(\epsilon\log\epsilon)p_2-\epsilon\left\{\Omega p_2+\omega_{20}\left[\tfrac{1}{4}\left(y-\int_{-\infty}^x p_2\,dx\right)^2+p_2\log y\right]\right\}\ , \tag{44}$$

where

$$p=p_2+\epsilon p_3\ , \tag{45}$$

and

$$\omega_{20}=2\xi C^{1/8}\lambda^{1/4}(M_\infty^2-1)^{-1/8}(T_w^*/T_\infty^*)^{1/2}\ , \tag{46}$$

$$\Omega=-\alpha\phi C^{1/8}\lambda^{1/4}(M_\infty^2-1)^{-1/8}\left(\frac{T_w^*}{T_\infty^*}\right)^{1/2}+2^{1/2}C^{1/8}\lambda^{5/4}\times\left(\frac{T_w^*}{T_\infty^*}\right)^{-1/2}(M_\infty^2-1)^{7/8}(I_1+\xi I_2)+\omega_{20}\{1+\log[2^{-1/2}C^{-1/8}\times\lambda^{-3/4}(M_\infty^2-1)^{-1/8}(T_w^*/T_\infty^*)^{1/2}]\}\ . \tag{47}$$

Similarly, matching the density gives

$$\rho\to 1-\frac{1}{2}\epsilon\omega_{20}\left(y-\int_{-\infty}^x p_2\,dx+\frac{p_2}{y}\right)\quad\text{as } y\to\infty\ . \tag{48}$$

We note that matching the transverse components of the velocities is redundant.

Equations (44), (45), and (48) suggest that the appropriate expansions in the lower deck should be

$$u=u_1+\epsilon\log\epsilon\,u_{20}+\epsilon u_{21}+\cdots, \tag{49}$$

$$v=v_1+\epsilon\log\epsilon\,v_{20}+\epsilon v_{21}+\cdots\ , \tag{50}$$

$$\rho=1+\epsilon\rho_2+\cdots, \tag{51}$$

$$p=p_2+\epsilon p_3+\cdots\ . \tag{52}$$

Substituting these expansions into the governing equations and equating coefficients of like powers of ϵ, we obtain

Order ϵ^0:

$$u_1\frac{\partial u_1}{\partial x}+v_1\frac{\partial u_1}{\partial y}=-\frac{dp_2}{dx}+\frac{\partial^2 u_1}{\partial y^2}\ , \tag{53}$$

$$\frac{\partial u_1}{\partial x}+\frac{\partial v_1}{\partial y}=0\ , \tag{54}$$

$$u_1=v_1=0\quad\text{at } y=0, \tag{55}$$

$$u_1\to y-\int_{-\infty}^x p_2\,dx\quad\text{as } y\to\infty\ , \tag{56}$$

$$u_1\to y\quad\text{as } x\to-\infty; \tag{57}$$

Order $\epsilon\log\epsilon$:

$$u_1\frac{\partial u_{20}}{\partial x}+v_1\frac{\partial u_{20}}{\partial y}+u_{20}\frac{\partial u_1}{\partial x}+v_{20}\frac{\partial u_1}{\partial y}=\frac{\partial^2 u_{20}}{\partial y^2}\ , \tag{58}$$

$$\frac{\partial u_{20}}{\partial x}+\frac{\partial v_{20}}{\partial y}=0\ , \tag{59}$$

$$u_{20} = v_{20} = 0 \quad \text{at } y = 0 , \tag{60}$$

$$u_{20} \to -\omega_{20} p_2 \quad \text{as } y \to \infty , \tag{61}$$

$$u_{20} \to 0 \quad \text{as } x \to -\infty ; \tag{62}$$

Order ϵ:

$$u_1 \frac{\partial u_{21}}{\partial x} + v_1 \frac{\partial u_{21}}{\partial y} + u_{21} \frac{\partial u_1}{\partial x} + v_{21} \frac{\partial u_1}{\partial y}$$

$$= -\frac{dp_3}{dx} + \frac{\partial^2 u_{21}}{\partial y^2} - \rho_2 \left(-\frac{dp_2}{dx} + \frac{\partial^2 u_1}{\partial y^2} \right) - \frac{\partial}{\partial y} \left(\rho_2 \frac{\partial u_1}{\partial y} \right) , \tag{63}$$

$$\frac{\partial u_{21}}{\partial x} + \frac{\partial v_{21}}{\partial y} = -\frac{\partial \rho_2}{\partial y} , \tag{64}$$

$$u_1 \frac{\partial \rho_2}{\partial x} + v_1 \frac{\partial \rho_2}{\partial y} = \frac{\partial^2 \rho_2}{\partial y^2} , \tag{65}$$

$$u_{21} = v_{21} = \rho_2 = 0 \quad \text{at } y = 0, \tag{66}$$

$$u_{21} \to -\Omega p_2 - \omega_{20} \left[\tfrac{1}{4} \left(y - \int_{-\infty}^{x} p_2 \, dx \right)^2 + p_2 \log y \right] \quad \text{as } y \to \infty, \tag{67}$$

$$\rho_2 \to -\tfrac{1}{2} \omega_{20} \left(y - \int_{-\infty}^{x} p_2 \, dx + \frac{p_2}{y} \right) \quad \text{as } y \to \infty , \tag{68}$$

$$u_{21} \to -\tfrac{1}{4} \omega_{20} y^2, \quad \rho_2 \to -\tfrac{1}{2} \omega_{20} y \quad \text{as } x \to -\infty. \tag{69}$$

The equations pertinent to the case of an insulated wall are readily obtained from the present solution by setting $\xi \equiv 0$.

The three problems defined here could be solved in succession. The following scheme is followed for the case of constant wall temperature. The leading-order terms u_1, v_1, and p_2 are determined first by solving Eqs. (53)–(57). In fact, the first-order theory does not depend on the thermal condition of the wall. The next step is to solve for ρ_2 from Eqs. (65), (66), and (68). With the density ρ_2 known, we do not have to solve the problems for $O(\epsilon \log \epsilon)$ and $O(\epsilon)$ separately. Instead, we consider Eqs. (40) and (42) which govern the total values of u, v, and p. When dealing with the matching condition (44), we consider $p_2(x)$ to be known, but p is still unknown. This procedure enables one to use the same computer program to solve for both the leading-order terms as well as the second-order terms with some modifications in the boundary conditions.

We note that further simplifications are possible in the case of adiabatic walls since the terms $O(\epsilon \log \epsilon)$ are identically zero and $\rho = 1 + O(\epsilon^2)$. Therefore, the governing equations in the lower deck become the incompressible boundary-layer equations subject to

$$u = v = 0 \quad \text{at } y = 0 , \tag{70}$$

$$u \to y - \int_{-\infty}^{x} p \, dx - \epsilon \Omega p_2 \quad \text{as } y \to \infty , \tag{71}$$

$$u \to y \quad \text{as } x \to -\infty. \tag{72}$$

Since $p = p_2 + \epsilon p_3$, Eq. (71) can be rewritten as

$$u \to y - \int_{-\infty}^{x} p \, dx - \epsilon \Omega p \quad \text{as } y \to \infty, \tag{73}$$

where a term $O(\epsilon^2)$ is neglected, which is consistent with the order of the theory presented here. Now, if Eq. (73) is used in place of Eq. (71), one can obtain the total second-order solution for the lower-deck equations without solving for the leading-order terms. Again, the same computer program that solves the leading-order terms can easily be modified to account for the additional term $\epsilon \Omega p$ in the matching condition.

It is worth noting that the modified matching condition has the same form as in the hypersonic triple-deck theory if $\epsilon \Omega$ is interpreted as the hypersonic parameter σ of Ref. 13; however, the physical content of these terms is different.

IV. NUMERICAL METHOD AND APPLICATION TO THE COMPRESSION RAMP

Jenson *et al.*,[6] Rizzetta,[7] and Rizzetta *et al.*[8] used the first-order theory to determine the flow over a compression ramp with small-bubble separation. The angle of the ramp is $O(\epsilon^2)$; a necessary condition for the separation bubble to be embedded in the lower deck. Prandtl's transposition theorem (e.g., Rosenhead[14]) was used to simplify the boundary conditions on the wall. New variables are introduced according to, see Fig. 2,

$$z = \begin{cases} y & \text{if } x < 0 , \\ y - \alpha x & \text{if } x \geq 0, \end{cases} \tag{74}$$

$$w = \begin{cases} v & \text{if } x < 0 , \\ v - \alpha u & \text{if } x \geq 0, \end{cases} \tag{75}$$

where α is related to the physical ramp angle α^* by

$$\alpha^* = [C \lambda^2 (M_\infty^2 - 1)]^{1/4} \epsilon^2 \alpha . \tag{76}$$

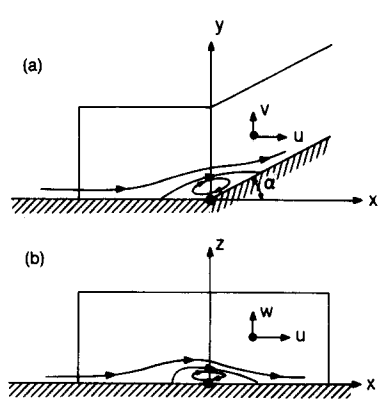

FIG. 2. The compression ramp; (a) physical coordinates and (b) transposed coordinates.

Now the reference point x_p^* is taken at the corner; that is, $x_p^* = x_c^*$, the distance from the leading edge to the start of the ramp.

As mentioned earlier, the main problem is to solve Eqs. (40) and (42) with ρ assumed known. In the transformed plane, these equations become

$$\rho\left(u\frac{\partial u}{\partial x}+w\frac{\partial u}{\partial z}\right)=-\frac{dp}{dx}+\frac{\partial}{\partial z}\left(\frac{1}{\rho}\frac{\partial u}{\partial z}\right), \tag{77}$$

$$\frac{\partial(\rho u)}{\partial x}+\frac{\partial(\rho w)}{\partial z}=0. \tag{78}$$

We eliminate $p(x)$ from Eq. (77) by differentiation with respect to z, use Eqs. (78) and (53), and obtain the equation

$$\frac{\partial\tau}{\partial t}+\rho u\frac{\partial\tau}{\partial x}+\rho w\frac{\partial\tau}{\partial z}=\frac{\partial^2}{\partial z^2}\left(\frac{\tau}{\rho}\right)-\epsilon F(x,z)+O(\epsilon^2\log\epsilon), \tag{79}$$

where

$$F(x,z)=\left(-\frac{dp}{dx}+\frac{\partial\tau_1}{\partial z}\right)\frac{\partial\rho_2}{\partial z}-\tau_1\frac{\partial^2\rho_2}{\partial z^2}, \tag{80}$$

$$\tau_1=\frac{\partial u_1}{\partial z}, \quad \tau=\frac{\partial u}{\partial z}. \tag{81}$$

Hence,

$$u=\int_0^z \tau\,dz. \tag{82}$$

We note that the unsteady form of the momentum equation is used. The inclusion of the term $\partial\tau/\partial t$ stabilizes the numerical procedure in the region of reversed flow.

A. The first-order problem (u_1, w_1, p_2)

The first-order problem is governed by Eqs. (78) and (79) with $\rho = 1$ and $F \equiv 0$. The appropriate boundary and matching conditions are

$$\tau_1 = 1 \quad \text{as } x \to \pm\infty, \tag{83}$$

$$\tau_1 = 1 \quad \text{as } z \to \infty, \tag{84}$$

$$\frac{\partial^2}{\partial x^2}\int_0^\infty \tau_1\,dz=\alpha\delta(x)-\left.\frac{\partial\tau_1}{\partial x}\right|_{z=0}, \tag{85}$$

where $\delta(x)$ is the Dirac-delta function. The last equation is obtained by differentiating Eq. (56) twice with respect to x and utilizing the momentum equation evaluated at the wall. The pressure $p_2(x)$ is obtained by integrating the equation

$$\frac{dp_2}{dx}=\left.\frac{\partial\tau_1}{\partial z}\right|_{z=0}. \tag{86}$$

B. The second-order density ρ_2

The problem governing the second-order density ρ_2 is

$$\frac{\partial\rho_2}{\partial t}+u_1\frac{\partial\rho_2}{\partial x}+w_1\frac{\partial\rho_2}{\partial z}=\frac{\partial^2\rho_2}{\partial z^2}, \tag{87}$$

$$\rho_2 = 0 \quad \text{at } z = 0, \tag{88}$$

$$\rho_2 \to -\frac{1}{2}\omega_{20}\left(z+\alpha x H(x)-\int_{-\infty}^{x} p_2\,dx+\frac{p_2}{z+\alpha x H(x)}\right) \text{ as } z\to\infty, \tag{89}$$

$$\rho_2 \to -\tfrac{1}{2}\omega_{20} z \quad \text{as } x\to-\infty, \tag{90}$$

where $H(x)$ is the unit step function; hence,

$$\rho = 1+\epsilon\rho_2. \tag{91}$$

C. The total solution: u, w, p

The pertinent equations are Eqs. (77) and (78) and the appropriate boundary and matching conditions are

$$\tau \to 1-\tfrac{1}{2}\epsilon\omega_{20} z \quad \text{as } x\to\pm\infty, \tag{92}$$

$$\tau \to 1-\tfrac{1}{2}\epsilon\omega_{20}\left(z+\alpha x H(x)-\int_{-\infty}^{x} p_2\,dx+2p_2[z+\alpha x H(x)]^{-1}\right) \quad \text{as } z\to\infty. \tag{93}$$

Equation (44) can be rewritten as

$$u \to z+\alpha x H(x)-\int_{-\infty}^{x} p\,dx+E(x,z), \tag{94}$$

where

$$E=-\omega_{20}(\epsilon\log\epsilon)p-\epsilon\Omega p_2+\epsilon\omega_{20}\left[\tfrac{1}{4}\left(z+\alpha x H(x)-\int_{-\infty}^{x} p_2\,dx\right)^2+p_2\log[z+\alpha x H(x)]\right] \tag{95}$$

is a known function. Differentiating Eq. (94) twice with respect to x yields

$$\frac{\partial^2}{\partial x^2}\int_0^\infty \tau\,dz\to\alpha\delta(x)-\frac{dp}{dx}+\frac{d^2E}{dx^2}. \tag{96}$$

Evaluating Eq. (77) at $z = 0$ gives

$$\frac{dp}{dx}=\left.\frac{\partial(\tau/\rho)}{\partial z}\right|_{z=0}. \tag{97}$$

hence,

$$\frac{\partial^2}{\partial x^2}\int_0^\infty \tau\,dz\to\alpha\delta(x)-\left.\frac{\partial\tau}{\partial z}\right|_{z=0}+\left.\frac{\partial^2E}{\partial x^2}\right|_{z\to\infty}. \tag{98}$$

Jenson *et al.*,[6] Rizzetta,[7] and Rizzetta *et al.*[8] solved for the leading-order terms using finite differences. The unknowns at the mesh points are $\partial\tau/\partial t$. All first x and z derivatives were evaluated by "windward differences" and all second derivatives by centered differences. The truncation error in their work is $O(\Delta t, \Delta x, \overline{\Delta z}^2)$ except for the compatibility condition (85) where the error is $O(\overline{\Delta x}^2)$. More details and extensive applications of the method were given by Rizzetta.[7] Reyhner and Flügge-Lotz[15] used the Crank–Nicolson finite-difference scheme in studying shock-wave/boundary-layer

interactions when a small separation bubble exists. In the region of reversed flow, the convective term $\rho u \times \partial u/\partial x$ in the momentum equation is either dropped completely or replaced by $0.1|\rho u|\partial u/\partial x$. This results in a stable forward-marching procedure for reversed flows.

In the present work, the latter scheme is used, but the convective term $\rho u\, \partial \tau/\partial x$ is retained without change. Since the steady-state solution is achieved by marching in time as well as in space, the resulting tridiagonal system of equations is made diagonally predominant in the region of reversed flow by suitably choosing the time interval Δt for fixed Δx, Δz, and α. Diagonal dominance is a sufficient condition for the round-off error not to grow in the Thomas algorithm; this point is discussed in Ref. 16.

Finally, we note that the numerical treatment of the upstream and downstream matching conditions

$$\tau \to 1 \quad \text{as } x \to \pm\infty$$

is the same as that in Ref. 7 where an asymptotic solution valid for large $\pm x$ is utilized. The initial guess for the first-order problem (i.e., the values at time $t = 0$) is $\tau = 1$ everywhere in the domain of solution. Then, the first-order solution is used as the initial guess for the total second-order problem.

V. RESULTS AND DISCUSSION

To show that the finite-difference scheme is second-order accurate in the step size Δx, we obtained numerical results to the first-order problem for the flow over a compression ramp with $\alpha = 2.5$. Figure 3 shows the pressure and the wall shear stress at $x = -4.8$ as a function of $\overline{\Delta x}^2$. The figure clearly shows that the error is proportional to $\overline{\Delta x}^2$. The same trend was found for other points on the boundary as well as points inside the computational field. Also, the same results are plotted in Fig. 4 against Δx along with results of the first-order scheme used by Rizzetta *et al.*[8] Linear extrapolation to a zero step size of the results of Ref. 8 is necessary to obtain agreement with the present scheme at finite Δx.

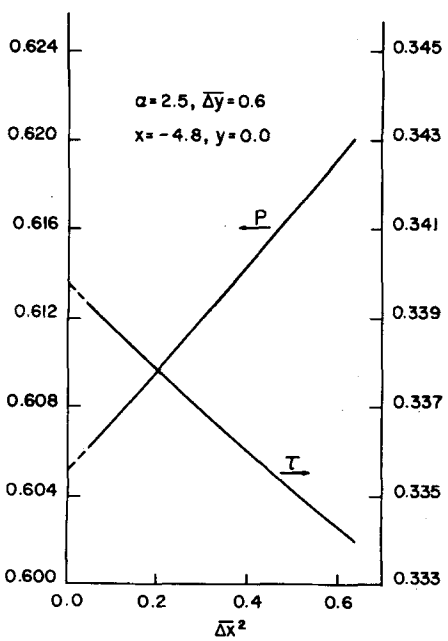

FIG. 3. Dependence of the pressure and wall shear on $(\Delta x)^2$ at $x = -4.8$.

The pressure and shear distributions for adiabatic walls predicted by the first- and second-order theories are shown in Figs. 5 and 6. Also, Carter's solution[10] of the Navier–Stokes equations is plotted in terms of the lower-deck variables. We note that the second-order theory predicts a smaller free-interaction region. Both the first- and second-order theories are in poor agreement with the solution of the Navier–Stokes equations. Far upstream, the viscous hypersonic interaction is pronounced; a factor that is not accounted for in the present theory. Far downstream the pressure predicted by the triple-deck theory approaches the inviscid linearized value, which is expected since in the upper deck the disturbance quantities are governed by the linearized supersonic potential-flow equations; a fact that is imposed by the scaling of the variables in that deck.

Brown and Williams[12] developed a second-order theory to study free interactions for the case of an adiabatic wall. They gave the following expression for the pressure and its x derivative at the new point of separation:

$$p = 1.026 - 0.228\,\epsilon\Lambda + O(\epsilon^2)\,, \tag{99}$$

$$p' = 0.263 + 0.45\,\epsilon\Lambda + O(\epsilon^2)\,, \tag{100}$$

where $\Lambda = \Omega/\sqrt{2}$. Based on the present calculations, the corresponding expressions are

$$p = 1.026 - 0.295\,\epsilon\Lambda + O(\epsilon^2)\,, \tag{101}$$

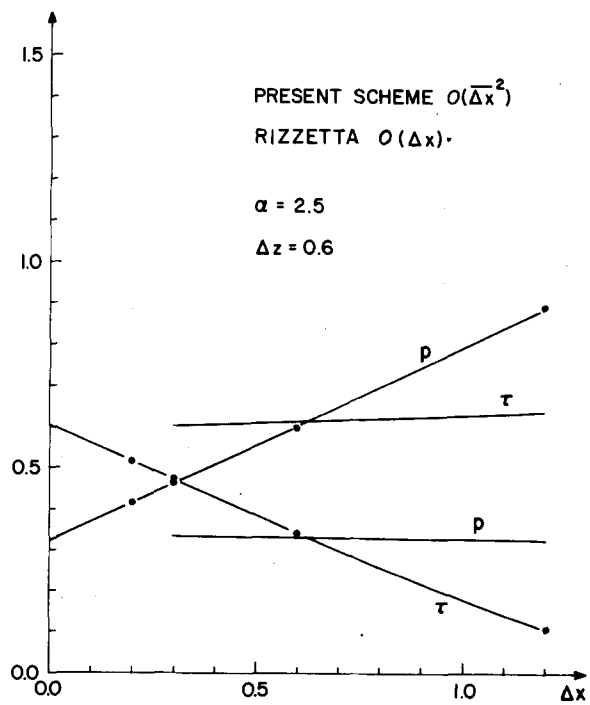

FIG. 4. Dependence of the pressure and wall shear stress on the step size Δx at $x = -4.8$.

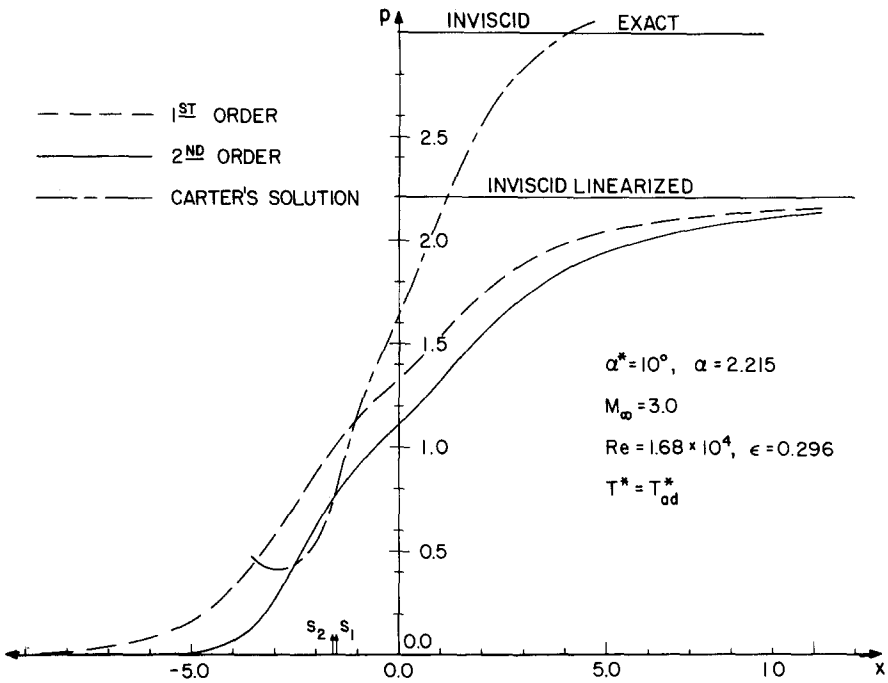

FIG. 5. Pressure distribution for an adiabatic wall.

$$p' = 0.263 + 0.031\ \epsilon\Lambda + O(\epsilon^2)\ . \qquad (102)$$

The numerical factors in Eqs. (101) and (102) were found as follows: First, the first-order problem for a compression ramp for $\alpha = 2.2$ was calculated. At the point of separation we found $p_1 = 1.026$ and $p_1' = 0.263$. Second, the total second-order solution was obtained for $\epsilon\Lambda = 0.05$ and 0.1; and p_2 and p_2' were determined at the point of separation. Using these values and the first-order value (i.e., $\epsilon\Lambda = 0$), we expressed p_2 and p_2' as quadratic functions of $\epsilon\Lambda$. The first two terms in these functions are shown in Eqs. (101) and (102). Comparison of these expressions shows that the corrections to p and p' are far away, especially those for p'.

Results for a cold wall are shown in Figs. 7 and 8 along with the solution of Werle and Vatsa[9] obtained by integrating the interacting boundary-layer equations, taken from Ref. 11. It is obvious that the trend predicted using the second-order theory is in the wrong direction. This is so because Davis and Werle[17] showed that solutions obtained by using the interacting boundary-layer equations agree very well with experimental data.

The reason for this discrepancy is attributed to the expansion of the basic-flow quantities in Taylor series in terms of the transverse coordinate, which is valid only for small values of the argument. For example,

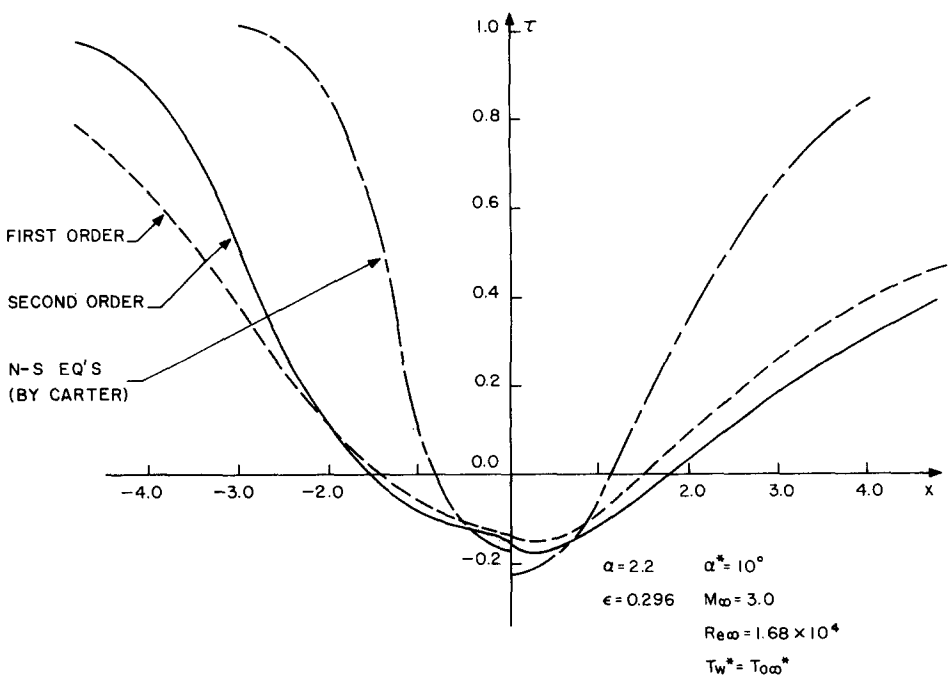

FIG. 6. Stress distribution for an adiabatic wall.

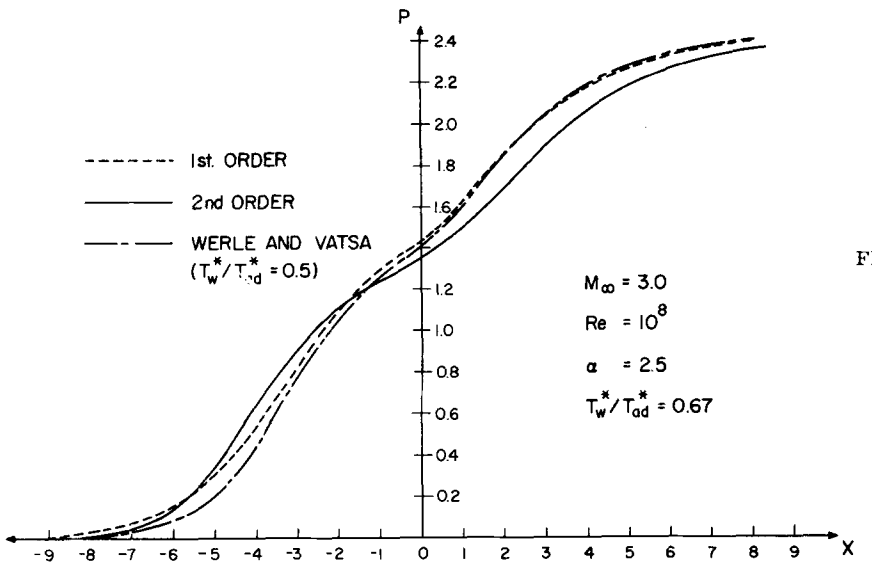

FIG. 7. Pressure distribution for a cooled wall.

the density and velocity profiles, $R(Y_m)$ and $U(Y_m)$, were expanded as

$$R(Y_m) = R(0) + \frac{dR(0)}{dY_m} Y_m + O(Y_m^2) ,$$

$$U(Y_m) = \frac{dU(0)}{dY_m} Y_m + \frac{1}{2} \frac{d^2U(0)}{dY_m^2} Y_m^2 + O(Y_m^3) .$$

For an adiabatic wall, $R'(0)$ and $U''(0)$ are zero, while they take negative values for cold walls. The expansions were used to evaluate the behavior of the solution in the main deck as $Y_m \to 0$, and the expressions thus obtained serve as the boundary conditions for the solution in the lower deck as $Y_l \to \infty$. Since $Y_l = Y_m/\epsilon$, the matching process implies that ϵ has to be very small; otherwise, Y_m will be large and hence truncating the Taylor series after two terms will not be valid. Figures 9 and 10 show the exact density and velocity profiles and their approximations by using one or two terms of the Taylor series. The results are plotted in terms of the transformed lower-deck variables, Eq. (39). Numerical results of the first-order terms show that the value of y which can be accepted as infinity is not less than 14, especially in the region of reversed flow. When we use this value in the second-order theory, the computational process either blows up or predicts incorrect results due to small or negative values of the density.

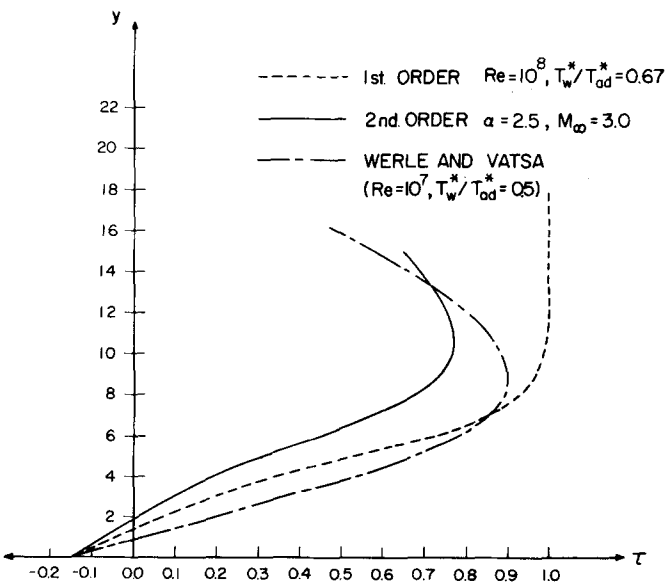

FIG. 8. Shear profile at the corner for a cool wall.

Since the first-order equations do not depend explicitly on the flow parameters, a numerical solution can always be obtained without assigning specific values to the Reynolds number, Mach number, and the wall temperature. The practicality of the solution thus obtained will depend on the values of the flow variables to be assigned. Using the present method for cooled walls requires assigning numerical values to the flow parameters. If these values are outside the range of validity of the asymptotic expansion, the nonuniformity might manifest itself in the course of computation in the form of very small or negative densities.

VI. CONCLUDING REMARKS

The method of matched asymptotic expansions is used to determine the second-order terms in the triple-deck theory for the case of constant wall temperature. The adiabatic wall equations are included as a special case. The Crank–Nicolson finite-difference scheme is used to obtain numerical solutions of the governing equations. Comparing these numerical solutions with those obtained by integrating the full Navier–Stokes equations or the interacting boundary-layer equations, we find that the first-order expansion is more accurate than the second-order expansion. Moreover, for the case of cooled walls, we find that the second-order expansion may predict negative densities and temperatures, depending on the Reynolds number and the degree of cooling, indicating a breakdown of the matched-asymptotic-expansion version of the triple-deck theory.

To understand the cause of this breakdown, we review the major assumptions underlying the triple-deck

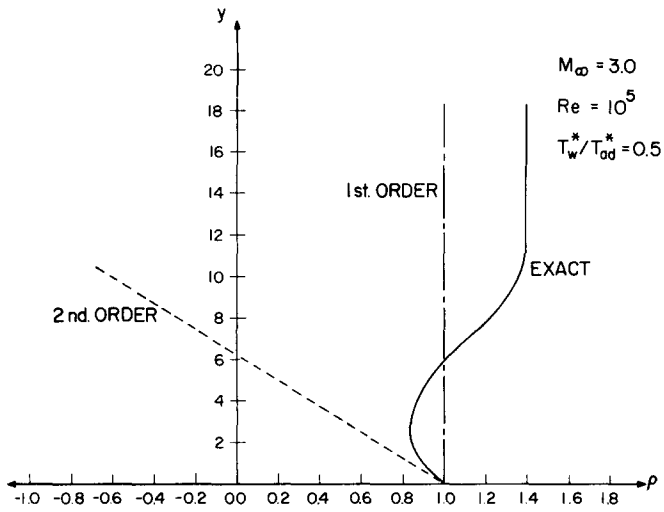

FIG. 9. Approximation to the basic density profile.

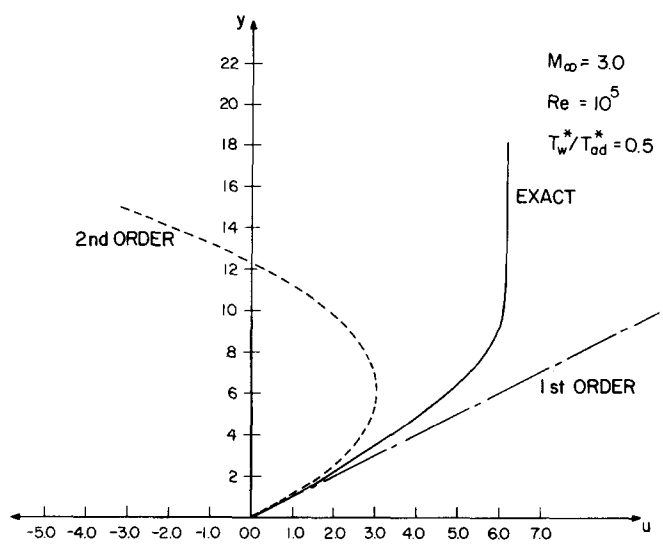

FIG. 10. Approximation to the basic velocity profile.

theory. First, the basic flow is assumed to be parallel, and hence stream-tube divergence in the middle deck is neglected. This assumption seems to be justifiable since the rate of change of the basic flow with the streamwise position is third order and hence it is the order of the neglected terms. This view is not shared by Tu and Weinbaum,[18] who suggested that the poor agreement between the first-order triple-deck theory and their nonasymptotic theory is mainly due to the parallel-flow assumption. Second, in the matched-asymptotic-expansion version of the triple-deck theory, the basic flow and the other terms in the middle-deck solution are expanded in powers of the transverse coordinate for matching with the lower-deck solution. This assumption is justifiable only if the Reynolds number is very high so that the lower deck lies in a region in which the basic profiles are quadratic functions of the transverse coordinate. Third, the scaling laws in the upper deck dictate the use of the linearized supersonic-flow equations which underpredict the pressure. We note that none of these assumptions was used in the interacting boundary-layer model[9] or the nonasymptotic solution of Tu and Weinbaum.[18]

It seems that the greatest weakness in the matched-asymptotic-expansion version of the triple-deck theory is the expansion of the basic flow in powers of the transverse coordinate. Although the effect of the stream-tube divergence is third order, it may not be negligible for moderate Reynolds numbers because ϵ is not very small. The effects of stream-tube divergence can be included in an analysis based on the method of multiple scales[19] by at least considering the basic flow to be quasi-parallel.

ACKNOWLEDGMENTS

The discussion with Dr. R. T. Davis is greatly appreciated.

This work was supported by the Fluid Dynamics Program of the United States Office of Naval Research.

[1]M. J. Lighthill, Proc. R. Soc. London Ser. A **217**, 478 (1953).
[2]K. Stewartson and P. G. Williams, Proc. R. Soc. London Ser. A **312**, 181 (1969).
[3]V. Y. Neiland, Mekh. Zh. Gaza **4**, 40 (1969).
[4]A. F. Messiter, SIAM J. Appl. Math. **18**, 241 (1970).
[5]K. Stewartson, Adv. Appl. Math. **14**, 145 (1974).
[6]R. Jenson, O. R. Burggraf, and D. P. Rizzetta, in *Proceedings of the 4th International Conference on Numerical Methods in Fluid Mechanics* (Springer-Verlag, New York, 1975), Vol. 35, p. 218.
[7]D. P. Rizzetta, Ph.D. dissertation, The Ohio State University (1976).
[8]D. P. Rizzetta, O. R. Burggraf, and R. Jenson, J. Fluid Mech. **89**, 535 (1978).
[9]M. J. Werle and V. N. Vatsa, AIAA J. **12**, 1491 (1974).
[10]J. E. Carter, Ph.D. dissertation, Virginia Polytechnic Institute and State University (1971).
[11]O. R. Burggraf, D. P. Rizzetta, M. J. Werle, and V. N. Vatsa, AIAA J. **17**, 336 (1979).
[12]S. N. Brown and P. G. Williams, J. Inst. Math. Appl. **16**, 175 (1975).
[13]S. N. Brown, K. Stewartson, and P. G. Williams, Phys. Fluids **18**, 633 (1975).
[14]L. Rosenhead, *Laminar Boundary Layers* (Clarendon Press, Oxford, 1963), p. 211.
[15]T. A. Reyhner and I. Flügge-Lotz, Int. J. Non-Linear Mech. **3**, 173 (1968).
[16]J. E. Carter and S. F. Wornom, AIAA J. **13**, 1101 (1975).
[17]R. T. Davis and M. J. Werle, in *Proceedings of the 1976 Heat Transfer and Fluid Mechanics Institute* (Stanford University Press, Stanford, 1976), p. 317.
[18]K. Tu and S. Weinbaum, AIAA J. **14**, 767 (1976).
[19]A. H. Nayfeh, *Perturbation Methods* (Wiley, New York, 1973) (1973), Chap. 6.